Title

Complementary Interhelical Interactions between Three Buried Glu-Lys Pairs within Three Heptad Repeats Are Essential for Hec1-Nuf2 Heterodimerization and Mitotic Progression*

Journal

Journal of Biological Chemistry, 288(48)

ISSN

0021-9258

Authors

Ngo, Bryan
Hu, Chun-Mei
Guo, Xuning Emily
et al.

Publication Date

2013-11-01

DOI

10.1074/jbc.m113.490524

THE JOURNAL OF BIOLOGICAL CHEMISTRY VOL. 288, NO. 48, pp. 34403–34413, November 29, 2013

Complementary Interhelical Interactions between Three Buried Glu-Lys Pairs within Three Heptad Repeats Are Essential for Hec1-Nuf2 Heterodimerization and Mitotic Progression*[S]

Received for publication, June 2, 2013, and in revised form, October 11, 2013 Published, JBC Papers in Press, October 15, 2013, DOI 10.1074/jbc.M113.490524

Bryan Ngo, Chun-Mei Hu, Xuning Emily Guo, Brittany Ngo, Randy Wei, Jiewen Zhu, and Wen-Hwa Lee[1]

From the Department of Biological Chemistry, School of Medicine, University of California, Irvine, California 92697

Background: Hec1 and Nuf2 are components of the NDC80 complex essential for faithful chromosome segregation.
Results: Three contiguous heptad repeats with buried interhelical Glu-Lys pairs are required for Hec1-Nuf2 dimerization, NDC80 complex formation, and mitotic progression.
Conclusion: Interhelical electrostatic and hydrophobic interactions define specificity and stability requirements for Hec1-Nuf2 dimerization.
Significance: The results elucidate how Hec1-Nuf2 dimerize and provide insight into NDC80 complex formation.

Hec1 and Nuf2, core components of the NDC80 complex, are essential for kinetochore-microtubule attachment and chromosome segregation. It has been shown that both Hec1 and Nuf2 utilize their coiled-coil domains to form a functional dimer; however, details of the consequential significance and structural requirements to form the dimerization interface have yet to be elucidated. Here, we showed that Hec1 required three contiguous heptad repeats from Leu-324 to Leu-352, but not the entire first coiled-coil domain, to ensure overall stability of the NDC80 complex through direct interaction with Nuf2. Substituting the hydrophobic core residues, Leu-331, Val-338, and Ile-345, of Hec1 with alanine completely eliminated Nuf2 binding and blocked mitotic progression. Moreover, unlike most coiled-coil proteins, where the buried positions are composed of hydrophobic residues, Hec1 possessed an unusual distribution of glutamic acid residues, Glu-334, Glu-341, and Glu-348, buried within the interior dimerization interface, which complement with three Nuf2 lysine residues: Lys-227, Lys-234, and Lys-241. Substituting these corresponding residues with alanine diminished the binding affinity between Hec1 and Nuf2, compromised NDC80 complex formation, and adversely affected mitotic progression. Taken together, these findings demonstrated that three buried glutamic acid-lysine pairs, in concert with hydrophobic interactions of core residues, provide the major specificity and stability requirements for Hec1-Nuf2 dimerization and NDC80 complex formation.

Faithful chromosome segregation is a highly dynamic process that depends on the precise interplay of spindle microtubules, kinetochores, motor proteins, kinases, and checkpoint proteins. Most notably, the four-protein kinetochore complex, NDC80, is essential for kinetochore-microtubule attachment and spindle assembly checkpoint signaling (1–6). EM studies have revealed that the NDC80 complex assembles into a 57-nm dumbbell-shaped rod with the central coiled-coil shaft flanked by the N-terminal globular heads of Hec1 (highly expressed in cancer 1) and Nuf2 and the C-terminal globular heads of Spc25 and Spc24 (3, 7). X-ray crystallography of an artificially shortened NDC80 complex (NDC80 Bonsai) lacking the coiled-coil domains has solved the structure of the globular heads, but not the full-length coiled-coil domains (8). Because of inherent difficulties in crystallizing the full-length NDC80 complex, high resolution structural details of the coiled-coil domains have yet to be elucidated. Therefore, alternative approaches are necessary to uncover important NDC80 functions assigned to this unresolved region.

Previous cross-linking experiments and mass spectrometry data have shed light on the organization and register of the Hec1 and Nuf2 coiled-coil domains (9). Using this combined approach, it was shown that there are four distinct positions along the parallel, intertwined coiled-coil domains of Hec1 and Nuf2 that are within close contact. In addition, using purified Hec1 and Nuf2 fragments, Ciferri *et al.* (10) demonstrated that the first coiled-coil domain of Hec1 could stably bind to the first coiled-coil domain of Nuf2, but not the second coiled-coil domain of Nuf2. This suggests that the coiled-coil domains may possess intrinsic specific motifs that determine Hec1-Nuf2 interaction specificity. Together, these studies suggest that the coiled-coil domains of Hec1-Nuf2 are essential for their dimerization. However, the critical elements responsible for their specific interaction have yet to be determined.

The hallmark structural feature of the coiled-coil is the seven-residue heptad repeat pattern, denoted as $(a\text{-}b\text{-}c\text{-}d\text{-}e\text{-}f\text{-}g)_n$. Hydrophobic amino acids are often present at the a and d "buried" positions every 3.6 residues, and polar/charged residues are at the adjacent flanking e and g "surface" positions (11–15). At this interval, a hydrophobic dimerization interface (core) is created, surrounded by interhelical electrostatic interactions

* This work was supported, in whole or in part, by National Institutes of Health Grant CA107568 (to W. H. L.).
[S] This article contains supplemental Fig. S1 and Table S1.
[1] To whom correspondence should be addressed: Dept. of Biological Chemistry, School of Medicine, University of California, Irvine, 240D Medical Sciences Bldg., Irvine, CA 92697-4037. Tel.: 949-824-4492; Fax: 949-824-9767; E-mail: whlee@uci.edu.

that may dictate protein interaction specificity. The remaining positions, b, c, and f, tend to be polar and form the helical surface exposed to the solvent environment (11, 14, 15). Among these positional parameters, the quaternary state of coiled-coil protein complexes are primarily determined by the nature of the residues in positions a, d, e, and g. Although there is a strong predilection for hydrophobic residues at the a and d positions, both polar and charged residues can be found at these positions. In fact, several studies have shown that these interior residues play a significant role in determining the quaternary structure of coiled-coil protein complexes (16–20). Thus, resolving how these positional preferences dictate Hec1-Nuf2 dimerization is critical for elucidating the overall process of NDC80 complex formation.

Because the first coiled-coil domain of Hec1 has been shown to interact with several mitotic proteins including Nek2, SMC1, Zwint1, and MSS1, in addition to Nuf2, it is predicted that the interaction mode for each binding partner can be varied (21–26). In this study, we set out to determine the requirements for Hec1-Nuf2 dimerization and whether this interaction is essential for NDC80 complex formation. We first generated a series of Hec1 deletion mutants, with each mutant removing two heptad repeat motifs along the first coiled-coil domain, and expressed them in cells. Our results demonstrated that Hec1 required three contiguous heptad repeats from Leu-331 to Leu-352, but not the entire first coiled-coil domain, to ensure overall stability of the NDC80 complex through direct interaction with Nuf2. Substituting the hydrophobic residues, Leu-331, Val-338, and Ile-345, of Hec1 with alanine completely eliminated Nuf2 binding and blocked mitotic progression. Furthermore, the Hec1-Nuf2 dimer relied on an atypical coiled-coil signature with an unusual distribution of charged residues within position d of the hydrophobic dimerization interface. Systematic mutational analysis revealed that Hec1-Nuf2 dimerization depends on three unique pairs of interhelical electrostatic interactions between a buried (d position) Hec1 glutamic acid patch (Glu-334, Glu-341, and Glu-348) and a surface (e position) Nuf2 lysine patch (Lys-227, Lys-234, and Lys-241). Mutating these corresponding d-e residues to alanine not only abolished the binding between Hec1 and Nuf2, but also reduced the overall stability of Spc25-Spc24 association and adversely affected mitotic progression. These results indicated that three consecutive heptad repeats, containing three buried charged residues, in concert with three hydrophobic core residues, provide the major specificity and stability requirements for Hec1-Nuf2 heterodimerization and NDC80 complex formation.

EXPERIMENTAL PROCEDURES

Antibodies—Commercial antibodies used for immunostaining or Western blotting were as follows: mouse monoclonal anti-Hec1 (9G3), mouse anti-β-actin, rabbit anti-CDCA1 (Nuf2), rabbit anti-Spc24, rabbit anti-Spc25 (GeneTex, Irvine, CA); rabbit anti-γ-tubulin and mouse anti-α-tubulin (Sigma-Aldrich); mouse anti-Nuf2 antibodies (MBL International, Woburn, MA); mouse anti-GFP monoclonal mixtures (Roche Applied Science); human anti-centromere antibody (Antibodies Inc., Davis, CA); and secondary antibodies conjugated with Alexa dyes (Invitrogen). Whenever possible, antibodies from different species were used for immunoprecipitation and immunoblotting experiments.

Plasmid Construction—Site-directed mutagenesis was performed on the RNAi-resistant pEGFP-N1-Hec1-GFP WT or pEGFP-N1-Nuf2-GFP WT constructs to create the desired mutations according to the instruction manual (Stratagene, La Jolla, CA). All constructs were validated by sequence analysis and subcloned into the pQXCIP6 retrovirus vector. PCR mutagenesis primers were synthesized by Integrated DNA Technologies (San Diego, CA). For a complete list of mutagenesis primers used, see supplemental Table S1.

Cell Culture and siRNA Knockdown—The human osteosarcoma cell line U2OS, the cervical cancer cell line HeLa, and the virus packaging cell line GP2–293 were cultured in DMEM supplemented with 10% heat-inactivated FBS and 1% penicillin-streptomycin at 37 °C under 10% CO_2. siRNA duplexes previously validated to target Hec1 and Nuf2 were custom-synthesized by Ambion (Austin, TX) and Dharmacon Research (Lafayette, CO), respectively. siRNA was transfected twice within 24 h into cells with Liopfectamine 2000 (Invitrogen) according to the manufacturer's protocol. Twenty-four hours after the last siRNA transfection, cells were fixed for microscopy or lysed for co-immunoprecipitation and/or Western blot analysis.

Retroviral Production Infection and Mitotic Index Measurement—Retroviral pQCXIP6 constructs, containing either Hec1 or Nuf2, were co-transfected into GP2–293 cells with a plasmid expressing G glycoprotein of the vesicular stomatitis virus, pVSV-G (Clontech). Virus was harvested 48 h post-transfection and used to infect U2OS cells. After four cycles of infections in 48 h, the mitotic index for cells expressing GFP-only, Hec1 WT, Nuf2 WT, or mutants was quantified from images taken by Nikon Alpha YS microscope (Nikon Instruments Inc., Melville, NY) and analyzed using ImageJ.

Immunoprecipitation and Western Blot Analysis—Cells at 80% confluency were treated with 200 ng/ml of nocodazole for 12 h before being harvested and lysed in 1 ml of lysis 250 buffer (50 mM Tris, pH 7.4, 250 mM NaCl, 5 mM EDTA, 5 mM EGTA, 0.1% Nonidet P-40, 50 mM NaF, 1 mM PMSF, and 1× proteinase inhibitor mixture; Roche Applied Science). Cell lysate was subjected to three liquid nitrogen freeze-thaw cycles and centrifuged at 16,000 rpm for 10 min at room temperature. Supernatant was removed and diluted to 125 mM NaCl. Lysate was preclarified by incubating with protein G-Sepharose (preblocked with 5% BSA for 3 h) for 1 h at 4 °C. For immunoprecipitation, clarified lysate was removed from beads and incubated with antibodies at 4 °C for 2 h, followed by incubation of fresh protein G-Sepharose beads for 6 h at 4 °C. Immunoprecipitates were washed five times with wash buffer (50 mM Tris, pH 7.4, 125 mM NaCl, 5 mM EDTA, 5 mM EGTA, 0.1% Nonidet P-40, 50 mM NaF, and 1 mM PMSF). The whole cell lysates and immunoprecipitates were separated by SDS-PAGE, transferred to Immobilon-P membranes (Millipore, Billerica, MA), and subjected to immunoblot analysis.

Immunofluorescence and Microscopy—Cells were grown on acid-etched coverslips and gently permeabilized with 0.5% Triton X-100 in PHEM buffer (80 mM PIPES, 25 mM HEPES, pH 7.2, 10 mM EGTA, 4 mM $MgSO_4$) for 5 min and subsequently

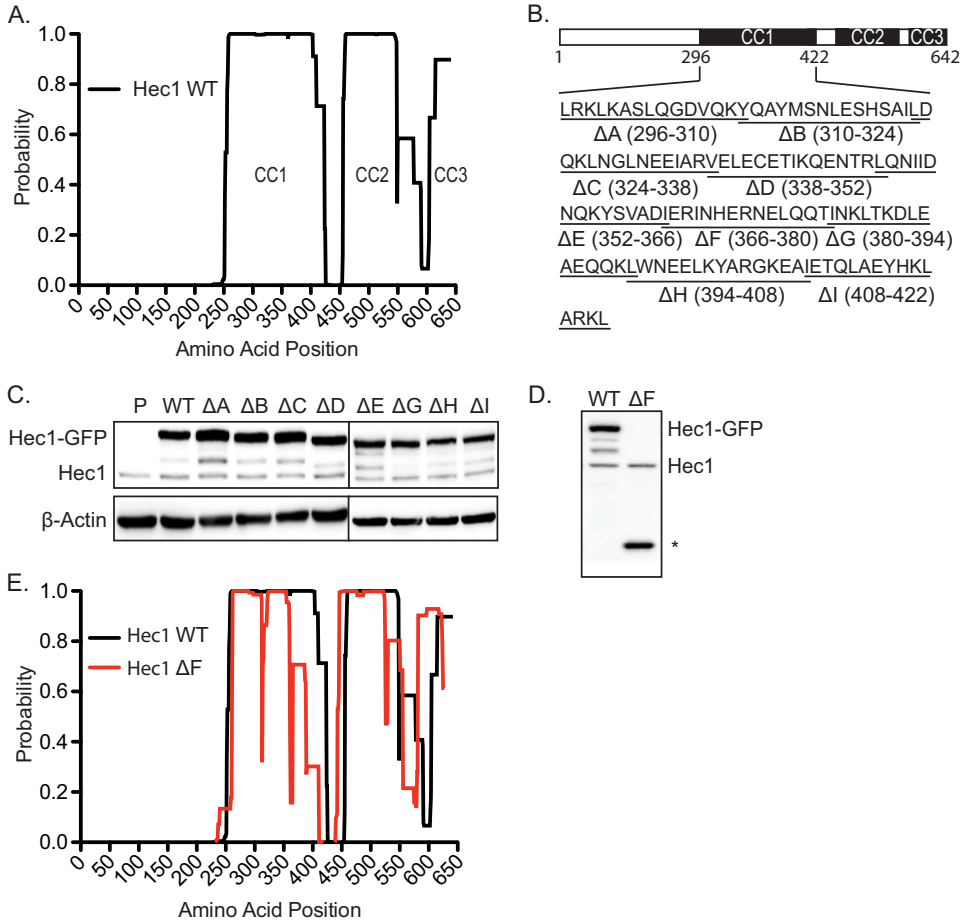

FIGURE 1. **Schematic diagram and expression of Hec1 deletion mutants.** *A*, Hec1 WT sequence was analyzed using the COILS algorithm. The probability of each residue contributing to coiled-coil formation was plotted as a function of its position within the overall sequence. *B*, schematic diagram illustrating the Hec1 deletion mutant constructs used in this study. The locations of the three coiled-coil domains are indicated in *black boxes* (CC1, CC2, and CC3). *C*, Western blot analysis of GP2–293 cells transfected with Hec1 WT or deletion mutants. β-Actin served as an internal loading control. *D*, Western blot analysis of GP2–293 cells transfected with Hec1 ΔF. *E*, Hec1 ΔF sequence was analyzed and compared with Hec1 WT using the COILS algorithm.

fixed for 20 min in PHEM buffer containing 4% paraformaldehyde (Electron Microscopy Sciences, Hatfield, PA). The cells were blocked with 5% normal goat serum in PHEM and then incubated with primary antibodies in phosphate-buffered saline overnight at 4 °C. Secondary antibodies used were conjugated with Alexa 555 or 546 (Molecular Probes, Invitrogen). Hoechst staining was applied after secondary antibody incubation, and cells were finally mounted on microscope slides with Prolong gold anti-fade reagent (Invitrogen). Images were captured using a Carl Zeiss Axiovert 200M motorized inverted microscope equipped with a Zeiss LSM 710 multispectral analyzer (Carl Zeiss Microscopy, Thornwood, NY). Serial sections of cells were acquired, and images were analyzed using ImageJ.

Internal Coordinate Mechanics Molecular Modeling—The Hec1-Nuf2 coiled-coil dimer model was built using GCN4 leucine zipper (Protein Data Bank code 2ZTA) as a structure template for α-carbon only. The alignment was then adjusted such that the residues of interest are aligned with the key hydrophobic residues of the leucine zipper. The Cartesian coordinates of the initial model were subsequently optimized and refined by side chain local minimization, until the protein health macro shows the energy strains of the majority of the residues are lower than 5 kcal/mol. All procedures were performed in ICM Pro (Molsoft LLC, San Diego, CA).

RESULTS

Generation of Deletion Mutants along the First Coiled-coil Domain of Hec1—To define and characterize the Hec1 coiled-coil region responsible for Nuf2 interaction, we first used the predictive software, COILS, to confirm the location of the Hec1 coiled-coil regions from its primary amino acid sequence (27). The COILS program compared the Hec1 sequence to a database of known parallel two-stranded coiled-coils and calculated the probability that the sequence will adopt a coiled-coil conformation. Meaningful coiled-coil scores provided by COILS predicted the presence of three coiled-coil domains in Hec1 (Fig. 1*A*). The first coiled-coil domain is the longest and spanned from amino acids 261 to 403. The second and third coiled-coil domains spanned from amino acids 458 to 570 and 597 to 642, respectively.

To experimentally address the role of this coiled-coil region in mediating Hec1-Nuf2 interaction, we generated a series of Hec1 deletion mutants spanning amino acids 296–422. For each mutant we used site-directed mutagenesis to systemati-

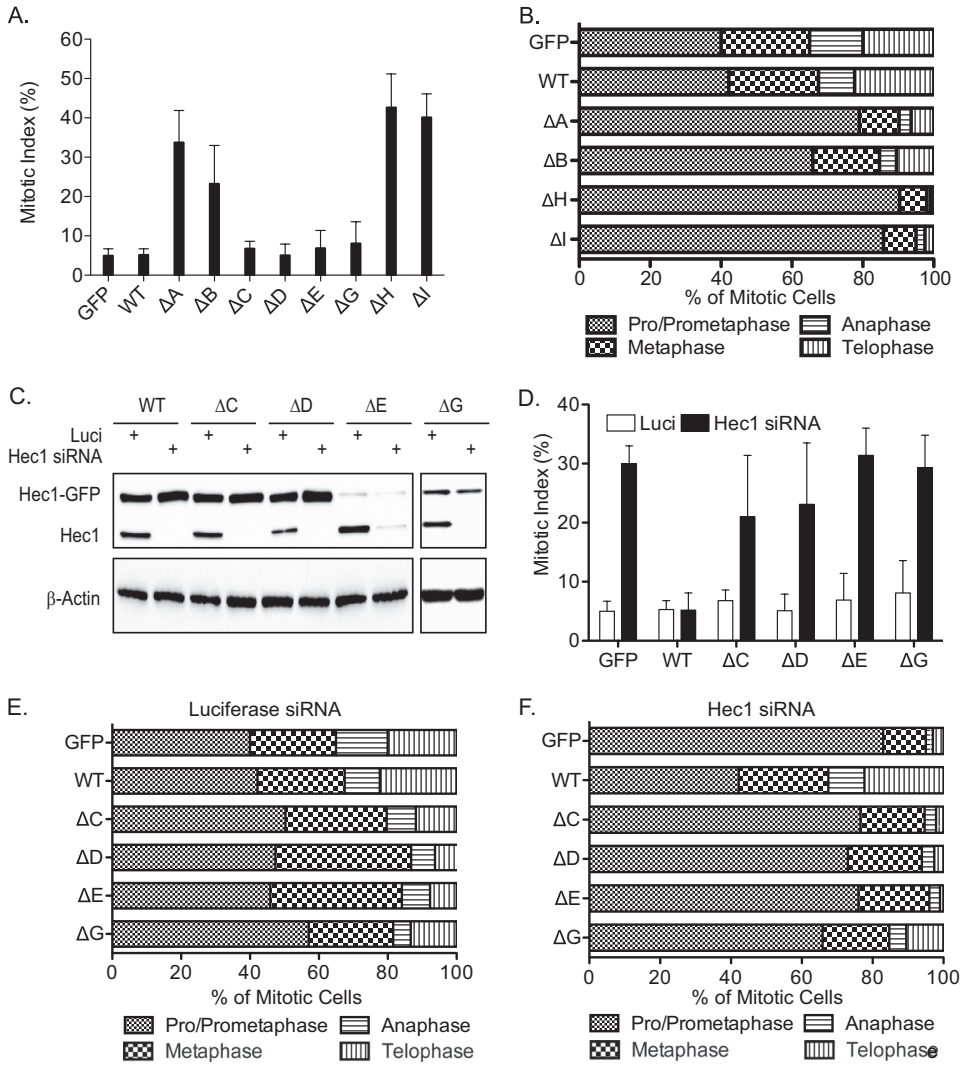

FIGURE 2. **Characterization of Hec1 deletion mutants.** *A*, mitotic index of U2OS cells ectopically expressing GFP-only, RNAi-resistant Hec1 WT, or Hec1 deletion mutants. Approximately 1,000 cells were collected for each sample from two separate experiments. *B*, mitotic distribution of U2OS cells expressing GFP-only, Hec1 WT, or dominant-negative Hec1 ΔA, ΔB, ΔH, and ΔI. *C*, Western blot analysis of U2OS cells with endogenous Hec1 depleted and expressing GFP-only, RNAi-resistant Hec1 WT, or nondominant-negative Hec1 ΔC, ΔD, ΔE, and ΔG. Luciferase siRNA was used as a negative control. β-Actin served as an internal loading control. *D*, mitotic index of U2OS cells ectopically expressing GFP-only, RNAi-resistant Hec1 WT, ΔC, ΔD, ΔE, or ΔG. Cells were either transfected with Hec1 siRNA or luciferase siRNA. Approximately 1,000 cells were counted for each sample from two separate experiments. *E* and *F*, mitotic distribution of U2OS cells expressing GFP-only, Hec1 WT, ΔC, ΔD, ΔE or ΔG with (*E*) or without (*F*) depletion of endogenous Hec1.

cally remove two consecutive heptad repeats along the first coiled-coil domain. These mutants were all generated using an RNAi-resistant pEGFP-Hec1-GFP WT construct as backbone and were sequenced verified prior to subcloning into a pQCXIP6-Hec1-GFP WT retrovirus vector. The resultant mutants were named ΔA through ΔI (Fig. 1*B*).

Next, we transiently transfected these deletion mutants into the virus packaging cell line, GP2–293. Western blot analysis showed that all Hec1 deletion mutants expressed at a level similar to Hec1 WT, except for Hec1 ΔF (Fig. 1*C*). Consistently, Hec1 ΔF was unable to be detected by Western blot, and visual inspection by fluorescence microscope showed little to no GFP expression in transfected GP2–293 cells (Fig. 1*D*). Analysis of the amino acid sequence for Hec1 ΔF using the COILS algorithm revealed a major distortion to the coiled-coil secondary structure in comparison with Hec1 WT, whereas the majority of the other truncation mutants showed no drastic deviation (Fig. 1*E* and supplemental Fig. S1). This raised the possibility that deletion of amino acids 352–381 could affect Hec1 protein conformation and stability. Therefore, Hec1 ΔF was excluded from subsequent experiments.

Analysis of the First Coiled-Coil Domain of Hec1 Essential for Mitotic Progression—To assess the consequence of the Hec1 deletion mutants to normal Hec1 function during mitosis, we carried out functional analyses on U2OS cells stably expressing GFP-only, Hec1 WT, or Hec1 deletion mutants. Following infection and selection, we examined the effect of these mutants on mitotic progression by calculating their respective mitotic indexes. As shown in Fig. 2*A*, cells expressing GFP-only or Hec1 WT resulted in a ~5% mitotic population. Cells expressing Hec1 ΔA, ΔB, ΔH, or ΔI resulted in mitotic arrest and exhibited a 3–4-fold increase in mitotic index, whereas cells expressing Hec1 ΔC, ΔD, or ΔE were able to complete mitosis and be propagated over many passages

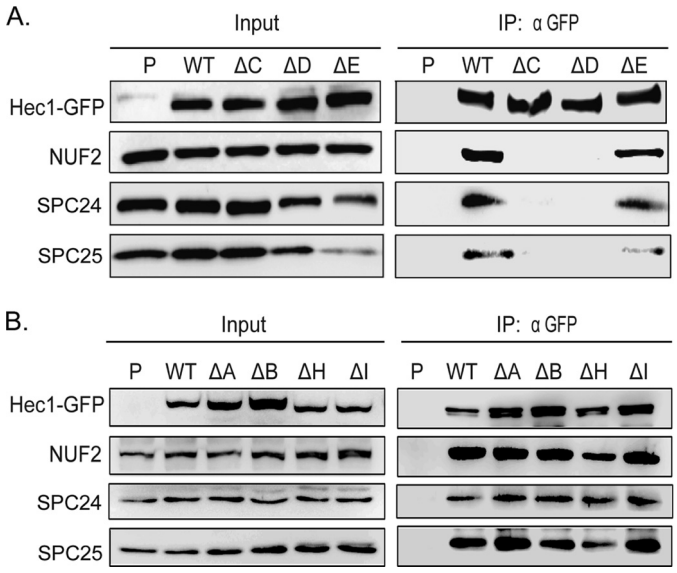

FIGURE 3. **Deletion of Hec1 amino acids 324–352 eliminates Hec1-Nuf2 interaction.** *A*, immunoprecipitation (*IP*) of Hec1 WT, ΔC, ΔD, or ΔE using anti-GFP antibody and Western blot analysis with GFP, Nuf2, Spc25, and Spc24 antibodies. *B*, immunoprecipitation of Hec1 WT, ΔA, ΔB, ΔH, or ΔI with anti-GFP antibody and Western blot analysis with GFP, Nuf2, Spc25, and Spc24 antibodies.

with no observable significant increase in mitotic index (Fig. 2, *A* and *B*).

To test whether endogenous Hec1 may mask the true phenotypes of Hec1 ΔC, ΔD, ΔE, and ΔG, U2OS cells stably expressing these mutants were transfected with Hec1 siRNA or luciferase siRNA (Fig. 2*C*). The mitotic population of these cells increased more than 4-fold when treated with Hec1 siRNA compared with luciferase siRNA-treated cells (Fig. 2*D*). Moreover, in contrast to the cells expressing Hec1 ΔA, ΔB, ΔH, or ΔI, where 65–85% of the mitotic cells were arrested in prometaphase, the mitotic distribution of cells expressing Hec1 ΔC, ΔD, and ΔE resembled that of cells expressing GFP-only or Hec1 WT without Hec1 siRNA treatment (Fig. 2*E*). Interestingly, when endogenous Hec1 was depleted, more than 65% of U2OS cells expressing Hec1 ΔC, ΔD, ΔE, or ΔG arrested in prometaphase with very few cells observed in anaphase and telophase (Fig. 2*F*). These results indicated that neither Hec1 ΔC, ΔD, ΔE, nor ΔG was able to rescue endogenous Hec1 function. Therefore, the dominant-negative phenotypes of Hec1 ΔA, ΔB, ΔH, and ΔI compared with nondominant-negative phenotypes of Hec1 ΔC and ΔD suggested that the different functions of Hec1 could be mediated through different regions along the first coiled-coil domain. These findings convey the possibility that the first coiled-oil domain of Hec1 may have a diverse range of functions.

Western blot analysis showed that Hec1 ΔE has low expression in infected U2OS cells but high expression in GP2–293 transfected cells (Figs. 1*C* and 2*C*). This suggested that high expression of Hec1 ΔE may not be compatible with cell survival. Therefore, only transfection of Hec1 ΔE was used in subsequent interaction experiments (Fig. 3*A*). In addition, Hec1 ΔG was excluded from additional experiments because the mitotic phenotype was ambiguous, and the mitotic distribution between siRNA treatment and luciferase treatment was not significant (Fig. 2, *A*, *E*, and *F*).

Deletion of Hec1 Amino Acid 324–352 Disrupts NDC80 Complex Formation—Although previous studies have demonstrated that Hec1 forms a heterodimer with Nuf2 through their respective coiled-coil domains (10), it is possible that certain heptads play a more significant role in mediating Hec1-Nuf2 dimerization than others. Therefore, the deletion of specific heptad repeats could weaken and/or disrupt Hec1-Nuf2 dimerization. As a result, the integrity of the NDC80 complex would be compromised and lead to aberrant mitosis. To test this possibility, we transfected HeLa cells with GFP-tagged Hec1 WT or Hec1 deletion mutants, and used anti-GFP antibody to immunoprecipitate Hec1-GFP from lysates of mitotically arrested HeLa cells. As shown in Fig. 3 (*A* and *B*), immunoblotting demonstrated that Nuf2, Spc25, and Spc24 co-immunoprecipitated with Hec1 WT, ΔA, ΔB, ΔE, ΔH, and ΔI, but not Hec1 ΔC and ΔD. This demonstrated that the majority of the first coiled-coil domain of Hec1 is not required for Nuf2 binding. Rather, Hec1-Nuf2 interaction appeared to depend on a short segment of Hec1 from amino acid 324 to 352. Additionally, dissociation of Hec1-Nuf2 also reduced Spc25 and Spc24 association, further suggesting that Hec1-Nuf2 interaction is required for overall NDC80 complex integrity (Fig. 3, *A* and *B*).

Buried Hec1 Glu-334, Glu-341, and Glu-348 Are Critical for Hec1-Nuf2 Interaction and Mitotic Progression—To further pinpoint the coiled-coil residues important for Hec1-Nuf2 interaction, we used DrawCoils to produce a helical diagram of the region deleted in Hec1 ΔC and ΔD (amino acid 324–352) (11). Intriguingly, despite the stereotypical coiled-coil structure of Hec1 324–352, the sequence of the interacting surface is rather unusual. Instead of having hydrophobic residues at both a and d positions, Hec1 324–352 contained a series of three highly conserved glutamic acid residues buried within the hydrophobic interface at position d: Glu-334, Glu-341, and Glu-348 (Fig. 4, *A* and *B*).

Previous studies have revealed that buried polar residues in coiled-coils can be important determinants of structural uniqueness and contribute to the stability of coiled-coil mediated interactions (28, 29). Therefore, it is possible that these glutamic acid residues serve an important function to specify the Hec1-Nuf2 heterodimer interaction and enhance the overall stability of the NDC80 complex. To precisely evaluate the importance of these highly conserved glutamic acid residues in Hec1 function, we generated three RNAi-resistant Hec1-GFP substitution mutants, in which the glutamic acid residues were replaced with alanine: Hec1 E341A (1EA), Hec1 E341A/E348A (2EA), and Hec1 E334A/E341A/E348A (3EA) (Fig. 4*C*).

Next, we tested whether these highly conserved glutamic acid residues were important for Hec1-Nuf2 association. Immunoprecipitation assay using mitotically arrested HeLa cell lysate expressing Hec1 WT, 1EA, 2EA, or 3EA confirmed that Hec1 2EA and 3EA showed drastically diminished Nuf2 binding compared with Hec1 WT (Fig. 4*D*). A reciprocal co-immunoprecipitation experiment using a Nuf2 antibody to pull down Nuf2-Hec1 complexes showed consistent results as endogenous Nuf2 showed a gradual reduction in binding affinity to

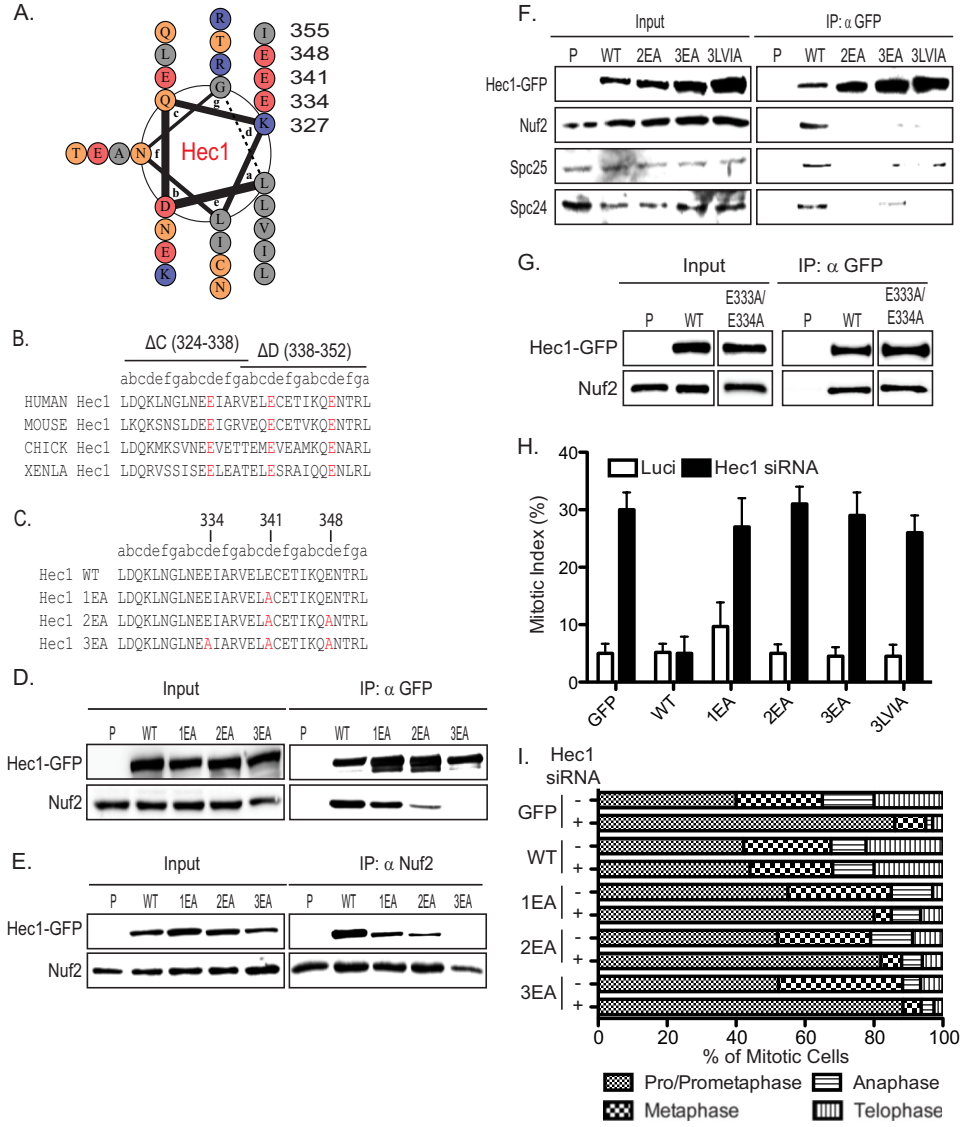

FIGURE 4. **Buried Hec1 Glu-334, Glu-341, and Glu-348 are critical for Hec1-Nuf2 interaction and mitotic progression.** *A*, a helical wheel representation of the Hec1 coiled-coil sequence, amino acids 324–355. Acidic charged residues are labeled in *red*, basic/positively charged residues are in *blue*, hydrophobic residues are in *gray*, and polar/uncharged residues are in *orange*. *B*, alignment of Hec1 coiled-coil sequence, amino acids 324–352, across the vertebrates. *Red letters* indicate the highly conserved glutamic acid residues. *C*, amino acid sequence of the three glutamic acid substitution mutants. *Red letters* indicate the site of alanine substitution mutation. *D*, immunoprecipitation of Hec1 WT, 1EA, 2EA, and 3EA with GFP antibody and Western blot analysis with GFP and Nuf2 antibodies. *E*, reciprocal immunoprecipitation of endogenous Nuf2 using a Nuf2 antibody in cells expressing Hec1 WT, 1EA, 2EA, or 3EA and Western blot analysis with GFP and Nuf2 antibody. *F*, immunoprecipitation of Hec1 WT, 2EA, 3EA, and 3LVIA using GFP antibody and Western blot analysis with GFP and Nuf2 antibodies. *G*, immunoprecipitation of Hec1 WT and E333A/E334A using GFP antibody and Western blot analysis with GFP and Nuf2 antibodies. *H* and *I*, mitotic index (*H*) and mitotic distribution (*I*) were measured in U2OS cells ectopically expressing GFP-only, RNAi-resistant Hec1 WT, 1EA, 2EA, or 3EA. Cells were either transfected with Hec1 siRNA (+) or luciferase siRNA (−). *IP*, immunoprecipitation; *Luci*, luciferase.

Hec1 1EA, 2EA, and 3EA (Fig. 4*E*). Taken together, these results suggested that the buried glutamic acid patch is important for Hec1-Nuf2 interaction and NDC80 complex formation.

To assess the contributions of hydrophobic mediated interaction *in vivo*, we mutated the hydrophobic residues Leu-331, Val-338, and Ile-345 at position a of the Hec1 helical wheel to alanine and tested whether abolishing these nonpolar residues (Hec1 3LVIA) would eliminate Hec1-Nuf2 interaction and disrupt NDC80 complex formation. As shown in Fig. 4*F*, substituting the hydrophobic residues within the same three heptad repeats dramatically diminished Hec1, Nuf2, Spc25, and Spc24 interaction. As a control, we also generated a Hec1 mutant with two Glu-333 and Glu-334 changed to alanine and assessed its ability to bind to Nuf2. Interestingly, mutating these residues did not appear to have a significant effect on Hec1-Nuf2 interaction (Fig. 4*G*). Therefore, for stable NDC80 complex association, Hec1 requires the contributions of both the buried glutamic acid residues Glu-334, Glu-341, and Glu-348 and the hydrophobic side chains Leu-331, Val-338, and Ile-345.

To determine whether these Hec1 glutamic acid residues were important for mitotic progression *in vivo*, we performed functional assays in U2OS cells infected with these glutamic acid substitution mutants. As shown in Fig. 4*H*, in the presence of endogenous Hec1, Hec1 WT, 2EA, and 3EA allowed normal mitosis and mitotic progression with minimal cytotoxicity. When endogenous Hec1 was depleted, a significant increase in

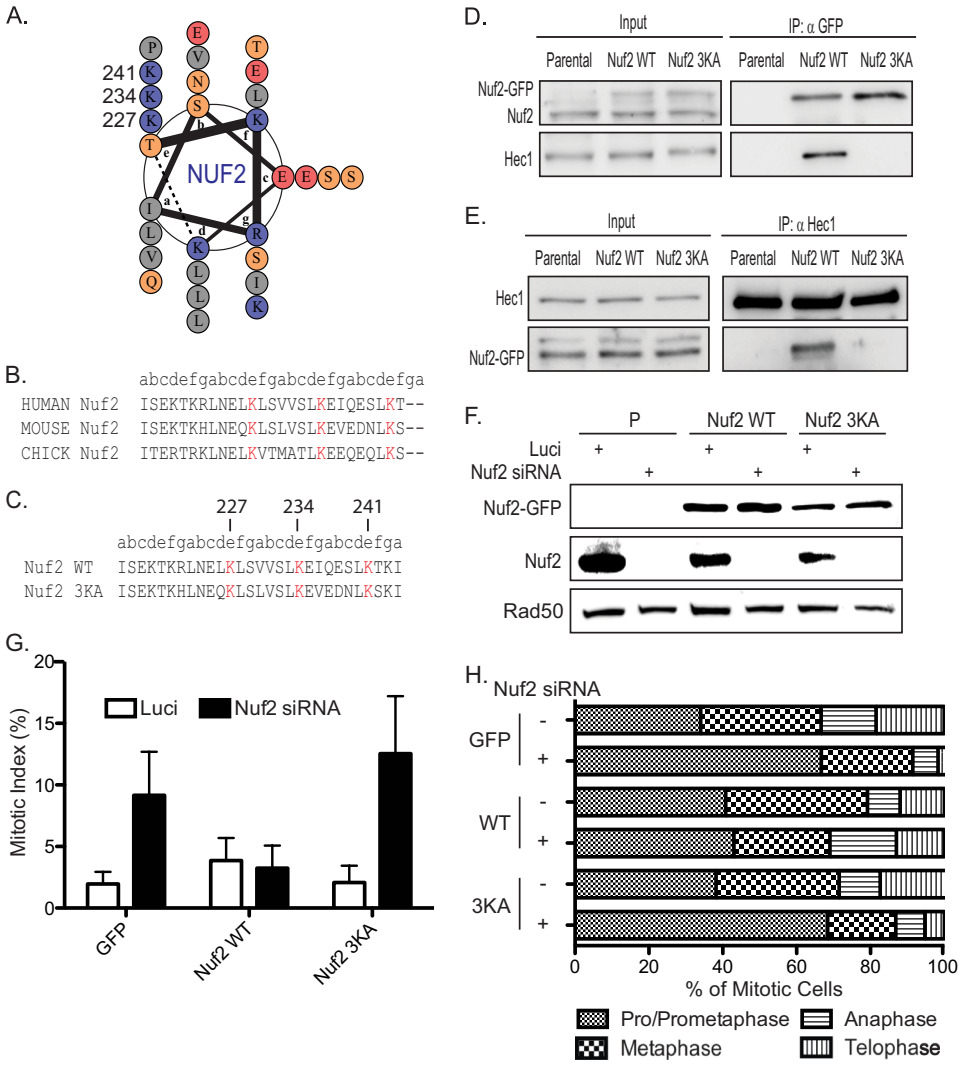

FIGURE 5. **Nuf2 Lys-227, Lys-234, and Lys-241 are essential for Nuf2-Hec1 interaction and mitotic progression.** *A*, a helical wheel representation of the Nuf2 coiled-coil sequence, amino acids 216–248. Acidic charged residues are labeled in *red*, basic/positively charged residues are in *blue*, hydrophobic residues are in *gray*, and polar/uncharged residues are in *orange*. *B*, alignment of Nuf2 coiled-coil sequence, amino acids 216–244, across the vertebrates. Sequences were aligned using UniProt Clustalo. *Red letters* indicate the highly conserved lysine residues. *C*, amino acid sequence of the Nuf2 K227A/K234A/K241A (Nuf2 3KA) substitution mutant. *Red letters* indicate the site of alanine substitution mutation. *D*, immunoprecipitation of Nuf2 WT and Nuf2 3KA with GFP antibody and Western blot analysis with GFP and Nuf2 antibody. *E*, reciprocal immunoprecipitation of endogenous Hec1 in cells expressing Nuf2 WT or Nuf2 3KA using a Hec1 antibody. *F*, Western blot analysis of U2OS cells ectopically expressing GFP-only, Nuf2 WT, or Nuf2 3KA. Luciferase siRNA was used as a control. Rad50 served as an internal loading control. *G* and *H*, mitotic index (*G*) and mitotic distribution (*H*) were measured in U2OS cells ectopically expressing GFP-only, Nuf2 WT, or Nuf2 3KA. Cells were treated with either Nuf2-siRNA (+) or luciferase siRNA (−) for 48 h. *IP*, immunoprecipitation; *Luci*, luciferase.

the mitotic index was observed in Hec1 1EA, 2EA, 3EA, and 3LVIA, but not Hec1 WT (Fig. 4*H*). Furthermore, cells expressing Hec1 1EA, 2EA, and 3EA all exhibited an 80% buildup of prometaphase cells upon depletion of endogenous Hec1, suggesting that these mutants were unable to rescue endogenous Hec1 (Fig. 4*I*). Altogether, these results suggested that the buried glutamic acid patch within the Hec1-Nuf2 dimerization interface serves a crucial role in mitotic progression.

Nuf2 Lys-227, Lys-234, and Lys-241 are Essential for Nuf2-Hec1 Interaction and Mitotic Progression—Because the surface potential of the Hec1 region required for Nuf2 binding is acidic (Hec1 amino acids 324–352), with an estimated pI value of 4.4 (full-length Hec1 is 5.4), it is possible that the interaction between Hec1 and Nuf2 may be based, at least in part, on electrostatic interactions. Under this scenario, we sought to align the coiled-coil registers of Hec1 and Nuf2 based on the cross-linking data to allow the cross-linked positions Hec1 Lys-360 and Nuf2 Lys-252 to be proximal to each other (9). Interestingly, we observed a stretch of basic lysine residues (Nuf2 Lys-227, Lys-234, and Lys-241) at the surface position e of the Nuf2 helical diagram, with a calculated pI value of 10.3 (full-length Nuf2 is 8.8) (Fig. 5, *A* and *B*). Therefore, it is plausible that Nuf2-Hec1 dimerization depends on a unique but highly conserved acid-base salt bridge interaction between the buried glutamic acid patch of Hec1 and a surface basic lysine patch of Nuf2 (Fig. 5*C*).

To validate this prediction, we generated a triple lysine Nuf2-GFP substitution mutant by replacing Lys-227, Lys-234, and Lys-241 with alanine. The resulting Nuf2 triple mutant was sequenced verified and called Nuf2 3KA (Fig. 5*C*). Next, we examined the ability of Nuf2 3KA to interact with Hec1 by pulldown experiments from mitotically arrested HeLa cell

lysate expressing Nuf2 WT or Nuf2 3KA. Using a GFP antibody to immunoprecipitate Nuf2-GFP WT and 3KA and immunoblotting with a Hec1 antibody, it was found that Nuf2 3KA failed to bind to Hec1 (Fig. 5*D*). Reciprocal co-immunoprecipitation experiment using a Hec1 antibody to immunoprecipitate endogenous Hec1 and immunoblotting against Nuf2 further confirmed that the Nuf2 lysine patch is required for interaction with Hec1 (Fig. 5*E*). Taken together, these results suggested that the corresponding interactions between the buried Hec1 glutamic acid patch and the Nuf2 lysine patch cooperatively mediated Hec1-Nuf2 heterodimerization.

To determine whether these Nuf2 lysine residues were important for mitotic progression *in vivo*, we expressed Nuf2 WT and 3KA in U2OS cells via retroviral infection and used the mitotic index and mitotic distribution profile as a functional measure. As shown in Fig. 5*G*, in the presence of endogenous Nuf2, U2OS Nuf2 WT and 3KA had normal mitotic indexes consistent with U2OS GFP-only cells (3–6%). When U2OS cells expressing GFP-only, Nuf2 WT, or Nuf2 3KA were depleted of endogenous Nuf2, U2OS GFP-only and Nuf2 3KA resulted in a 4–5-fold increase in the mitotic index, whereas Nuf2 WT was able to rescue cells depleted of endogenous Nuf2 (Fig. 5, *F* and *G*). Furthermore, cells expressing Nuf2 3KA exhibited a 70% accumulation of cells in prometaphase upon depletion of endogenous Nuf2, suggesting that this mutant was unable to substitute for endogenous Nuf2 (Fig. 5*H*). Altogether, these findings suggested that the surface lysine patch in Nuf2 serves a crucial role in mediating Hec1 interaction and mitotic progression.

Hec1-Nuf2 Dimerization Occurs through an Unusual Coiled-Coil Heptad Repeat Motif—Stereotypical coiled-coil proteins contain heptad repeats where the a and d positions are usually hydrophobic. However, contrary to this established arrangement, our results suggested that the Hec1-Nuf2 dimer depends on three buried glutamic acid residues at position d within the first coiled-coil domain of Hec1 and three complementary lysine residues in the first coiled-coil domain of Nuf2 at position e. Changing the buried glutamic acid patch in Hec1 or surface lysine residues in Nuf2 to alanine compromised both the Hec1-Nuf2 dimer formation and NDC80 complex stability. To precisely address the specificity of these residues, we swapped Hec1 glutamic acid residues for lysine residues (Hec13EK), and conversely Nuf2 lysine residues for glutamic acid residues (Nuf23KE), and asked whether these mutants retained Hec1-Nuf2 dimerization. To accomplish these goals, we co-immunoprecipitated Myc-tagged WT or 3KE Nuf2 from cells co-expressed with either GFP-tagged WT or 3EK Hec1 using anti-Myc antibody. As shown in Fig. 6*A*, cells expressed with both complementary charge-swapping mutants of Hec1 and Nuf2 retained Hec1-Nuf2 interaction, whereas cells expressed with either wild-type (Nuf2 WT; Hec1 WT) and mutant (Hec1 3EK; Nuf2 3KE) combinations abolished Hec1-Nuf2 binding (Fig. 6*A*).

After establishing the unique positional preferences of these buried charged interhelical residues, we used ICM-Pro to generate an optimized model of the Hec1-Nuf2 coiled-coil dimerization interface to support our hypothesis. Based on the crystal structure of the GCN4 leucine zipper transcription factor, ICM modeling revealed that heterodimerization between parallel Hec1 and Nuf2 coiled-coils is energetically feasible with both hydrophobic and electrostatic interactions contributing to the dimer formation (Fig. 6, *B*–*D*). The hydrophobic amino acids all point toward the central core of the heptad repeat, whereas the buried glutamic acid residues at position d of Hec1 are in close contact with the basic lysine residues of Nuf2 at position e. Moreover, the parallel Hec1-Nuf2 coiled-coil dimer is electrostatically favorable as oppositely charged side chains are brought into close juxtaposition (Fig. 6, *B*, *D*, and *E*). Taken together, the computer-generated models support the physical importance of both hydrophobic side chain interactions and interhelical electrostatic interactions between the buried glutamic acid residues of Hec1 and the surface lysine side chains of Nuf2.

DISCUSSION

In this communication, we have identified a novel buried interhelical electrostatic salt bridge essential for Hec1-Nuf2 dimerization, NDC80 complex formation, and mitotic progression. This process is dependent on an atypical coiled-coil signature, spanning three-heptad repeats within the first coiled-coil domain of Hec1, but not the full-length coiled-coil domain as previously reported. Instead of the stereotypical hydrophobic interactions between the adjacent a and d positions, the Hec1 coiled-coil region has charged glutamic acid residues at three d positions, which can form electrostatic interactions with the corresponding surface Lys residues on Nuf2 at the e position. Together with the hydrophobic interactions, these three complementary d-e electrostatic interactions lead to Hec1-Nuf2 dimerization and NDC80 complex formation.

Traditional coiled-coil proteins contain nonpolar residues at both the a and d positions to create a hydrophobic dimerization interface with the corresponding coiled-coil (11). Whereas the hydrophobicity is considered to be the major contributor to stable coiled-coil formation, as confirmed using the Hec1 3LVIA mutant (Fig. 4*F*), it is clear that buried surface d-e electrostatic interactions play an equally important role in determining the specificity and stability of coiled-coil association. Previously, Havranek and Harbury (30) discovered several new specificity motifs using an automated "multistate" method to uncover novel designs of specificity in coiled-coil proteins. One such novel design identified was the heterodimeric interaction between a buried glutamic acid residue at the d position and a surface arginine residue at the e position. This interaction signature was sufficient to specify a dimeric state at a significantly lower thermodynamic cost than the placement of two destabilizing residues with similar charges at the interacting interface. Likewise, the dimerization force dictated by the three complementary Glu-Lys pairs of Hec1-Nuf2, as described in our study, is consistent with this principle.

Interestingly, when we performed a similarity search using PATTINPROT, with the input heptad sequence (L/I/V/M)*XX*-E*XXX* repeated three times, to determine whether other coiled-coil proteins employ the same dimerization pattern, no other coiled-coil protein sequence was found, even when allowing for up to two mismatches (31). Thus, this highly unusual Hec1-Nuf2 interaction motif represents an extremely unique and important structural signature designed to dictate dimerization specificity.

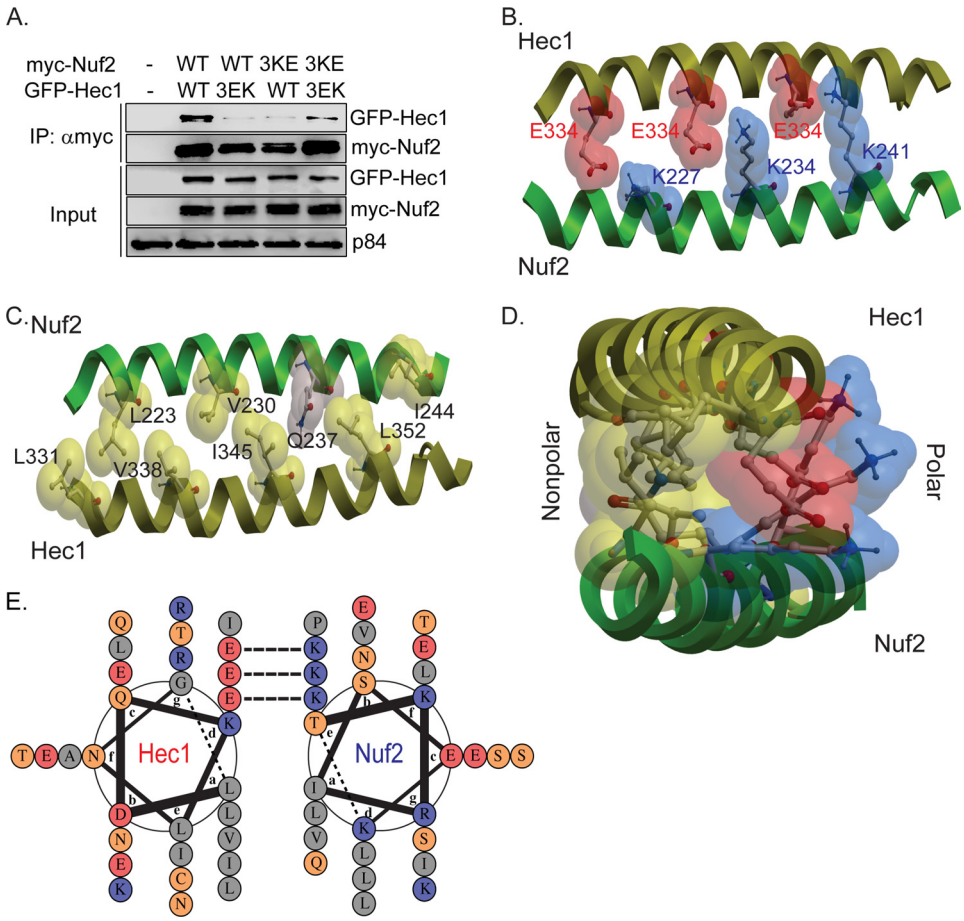

FIGURE 6. **Hec1-Nuf2 dimerization occurs through an unusual coiled-coil heptad repeat motif.** *A*, co-immunoprecipitation of either Myc-tagged WT or 3KE Nuf2 from cells co-expressed with either GFP-tagged WT or 3EK Hec1 using anti-Myc antibody. *B*, longitudinal view of an ICM-generated model of the parallel Hec-Nuf2 heterodimer showing the three interhelical electrostatic interactions between Hec1 Glu-334, Glu-341, and Glu-348 and Nuf2 Lys-227, Lys-234, and Lys-241. The N-terminal ends are on the *left-hand side*, and the C-terminal ends are on the *right-hand side*. *C*, longitudinal view of an ICM-generated Hec1-Nuf2 model showing the buried hydrophobic side chains of Hec1 Leu-331, Val-338, Ile-345, and Leu-352 and Nuf2 Leu-223, Val-230, and Ile-244. The N-terminal ends are on the *left-hand side*, and the C-terminal ends are on the *right-hand side*. *D*, cross-sectional view of an ICM-generated model of the parallel Hec1-Nuf2 heterodimer looking down the interhelical axis. Hec1 is shown as a *gold ribbon*, and Nuf2 is a *green ribbon*. The residues at the protein-protein interaction interface are shown as both ball-and-stick model and Core-Pauling-Koltun space filling model. The ball-and-stick atom model is colored according to atoms (*red*, oxygen; *blue*, nitrogen; *yellow*, carbon; *gray*, polar hydrogen). The Core-Pauling-Koltun space filling model is rendered transparent and colored according to the polarity of the residues (*yellow*, nonpolar; *red*, negatively charged; *blue*, positively charged; *purple*, neutral polar residues). *E*, a helical wheel diagram of amino acids 324–352 of Hec1 and amino acids 216–244 of Nuf2 showing the buried corresponding glutamic acid-lysine model of the Hec1-Nuf2 coiled-coil dimerization interface. Acidic charged residues are labeled in *red*, basic/positively charged residues are in *blue*; hydrophobic residues are in *gray*, and polar/uncharged residues are in *orange*. *IP*, immunoprecipitation.

Trigger sequences are autonomous helical folding modules that are critical for proper protein folding and complex formation (32–34). As shown here, the deletion of amino acids 366–380 (ΔF) resulted in an unstable Hec1 variant (Fig. 1*C*). Sequence analysis by the COILS algorithm confirmed that deletion of amino acid 366–380 (ΔF) abolished coiled-coil formation in one-third of the first coiled-coil domain of Hec1 (Fig. 1*E*). Interestingly, a sequence pattern search for the coiled-coil trigger sequence, (I/V/L)*X*(D/E)I*X*(R/K)*X*, matched the region deleted in Hec1 ΔF from amino acids Val-363 to Ile-369 with zero mismatches. Thus, deletion of this sequence may prevent proper coiled-coil formation, thereby resulting in a highly unstable Hec1 species that is rapidly degraded and presumably unable to dimerize with Nuf2 (Fig. 1*C*).

Dimerization of Hec1 and Nuf2 is critical for NDC80 complex formation, which also consists of SPC25 and SPC24. Previously, Ciferri *et al.* (10) showed that the full-length coiled-coil domains of Hec1 are not only important for Nuf2 interaction, but their association is regulated in a manner that enables the first coiled-coil domain of Hec1 to associate specifically with the first coiled-coil domain of Nuf2, but not the second. Based on our finding, Hec1-Nuf2 dimerization is dependent on an atypical coiled-coil signature, spanning only three-heptad repeats within the first coiled-coil domain of Hec1. This atypical coiled-coil structure contains three highly conserved buried glutamic acid residues at position d of the helical wheel diagram, Glu-334, Glu-341, and Glu-348, that can form interhelical electrostatic interactions with three corresponding surface e position Nuf2 lysine residues: Lys-227, Lys-234, and Lys-241. Changing these corresponding residues to alanine not only abolished the binding affinity between Hec1 and Nuf2, but also eliminated Spc25 and Spc24 interaction and compromised the overall stability of the NDC80 complex. Our results suggest that Hec1-Nuf2 dimerization precedes Spc25-Spc24 association and is essential for NDC80 complex formation. Whether addi-

tional regulation is involved to modulate NDC80 complex formation would be interesting to explore.

NDC80 complex plays an essential role in microtubule attachment and spindle assembly checkpoint signaling (1–6). Consistently, depletion of endogenous Hec1 or Nuf2 in cells expressing Hec1 3EA or Nuf2 3KA, respectively, reduced spindle assembly checkpoint molecules observed at the kinetochores and caused defects in chromosome congression. The inability of these cells to align their chromosomes may stem from unstable or improper kinetochore-microtubule attachments. These phenotypes are consistent with previous depletion experiments of other kinetochore components: Mis12, CENP-A, CENP-C, Spc24, and Spc25 (35–38). Likewise, these abnormalities may be a consequence of prolonged mitosis and compromised checkpoint functions.

Intriguingly, our systematic study showed that deletion of amino acids 296–324 (ΔA and ΔB) and 380–422 (ΔG, ΔH, and ΔI) resulted in dominant-negative prometaphase arrest, spindle abnormalities, and subsequent mitotic catastrophe (Fig. 2). Because all these deletion mutants were able to bind to Nuf2, except for Hec1 ΔC and ΔD, it suggested that different regions of the Hec1 coiled-coil can confer different functions. One possibility is that these heptad repeat subdomains are critical for Hec1 to interact with different mitotic proteins, and the disruption of these interactions may contribute to the dominant-negative prometaphase arrest phenotype. In fact, based on a yeast two-hybrid screen using the human Hec1 coiled-coil domain as bait, we identified Hice1, Nek2, SMC1, Zwint1, and MSS1 all as Hec1 interacting partners (21–26). The interactions between these proteins were independently confirmed, but the detailed binding mechanism remains unclear. It would be interesting to determine whether any of these deleted heptad repeats (ΔA, ΔB, ΔG, ΔH, and ΔI) are responsible for interacting with any of the aforementioned proteins (21–25). Establishing such direct interactions will enable us to precisely dissect the molecular mechanism of the dominant-negative prometaphase arrest phenotype.

Alternatively, these regions, Hec1 296–324 (ΔA and ΔB) and 380–422 (ΔG, ΔH, and ΔI), may contain potential post-translational modification site (*e.g.*, sumoylation) at the regions responsible for the dominant-negative phenotype. Proteomic screens in budding yeast have identified numerous kinetochore-associated proteins as sumoylation substrates, including Bir1p (homologue of Survivin), Sli15p (homologue of INCENP), and Mif2p (homologue of CENP-C) (39–44). Interestingly, recent studies have identified 14 potential sumoylation sites in the yeast homologue of Hec1, NDC80, of which K231 was found to be essential for NDC80 polysumoylation (29). Despite these findings, our understanding of human Hec1 sumoylation in the coiled-coil 1 region is lacking. Exploring whether these coiled-coil regions are targets for secondary modification may offer fascinating insight into Hec1 regulation and warrants further investigation.

Acknowledgments—We thank Dr. Jennifer DeLuca for the Nuf2-GFP construct used in this manuscript; Dr. Phang-Lang Chen, Dr. Yumay Chen, and Chi-Fen Chen for helpful experimental advice; and Andrew Lee and Hamilton Dang for technical support.

REFERENCES

1. DeLuca, J. G., Gall, W. E., Ciferri, C., Cimini, D., Musacchio, A., and Salmon, E. D. (2006) Kinetochore microtubule dynamics and attachment stability are regulated by Hec1. *Cell* **127,** 969–982
2. Guimaraes, G. J., Dong, Y., McEwen, B. F., and Deluca, J. G. (2008) Kinetochore-microtubule attachment relies on the disordered N-terminal tail domain of Hec1. *Curr. Biol.* **18,** 1778–1784
3. Wei, R. R., Al-Bassam, J., and Harrison, S. C. (2007) The Ndc80/HEC1 complex is a contact point for kinetochore-microtubule attachment. *Nat. Struct. Mol. Biol.* **14,** 54–59
4. Martin-Lluesma, S., Stucke, V. M., and Nigg, E. A. (2002) Role of Hec1 in spindle checkpoint signaling and kinetochore recruitment of Mad1/Mad2. *Science* **297,** 2267–2270
5. Alushin, G. M., Ramey, V. H., Pasqualato, S., Ball, D. A., Grigorieff, N., Musacchio, A., and Nogales, E. (2010) The Ndc80 kinetochore complex forms oligomeric arrays along microtubules. *Nature* **467,** 805–810
6. Wei, R., Ngo, B., Wu, G., and Lee, W. H. (2011) Phosphorylation of the Ndc80 complex protein, HEC1, by Nek2 kinase modulates chromosome alignment and signaling of the spindle assembly checkpoint. *Mol. Biol. Cell* **22,** 3584–3594
7. Wei, R. R., Sorger, P. K., and Harrison, S. C. (2005) Molecular organization of the Ndc80 complex, an essential kinetochore component. *Proc. Natl. Acad. Sci. U.S.A.* **102,** 5363–5367
8. Ciferri, C., Pasqualato, S., Screpanti, E., Varetti, G., Santaguida, S., Dos Reis, G., Maiolica, A., Polka, J., De Luca, J. G., De Wulf, P., Salek, M., Rappsilber, J., Moores, C. A., Salmon, E. D., and Musacchio, A. (2008) Implications for kinetochore-microtubule attachment from the structure of an engineered Ndc80 complex. *Cell* **133,** 427–439
9. Maiolica, A., Cittaro, D., Borsotti, D., Sennels, L., Ciferri, C., Tarricone, C., Musacchio, A., and Rappsilber, J. (2007) Structural analysis of multiprotein complexes by cross-linking, mass spectrometry, and database searching. *Mol. Cell. Proteomics* **6,** 2200–2211
10. Ciferri, C., De Luca, J., Monzani, S., Ferrari, K. J., Ristic, D., Wyman, C., Stark, H., Kilmartin, J., Salmon, E. D., and Musacchio, A. (2005) Architecture of the human ndc80-hec1 complex, a critical constituent of the outer kinetochore. *J. Biol. Chem.* **280,** 29088–29095
11. Grigoryan, G., and Keating, A. E. (2008) Structural specificity in coiled-coil interactions. *Curr. Opin. Struct. Biol.* **18,** 477–483
12. Cohen, C., and Parry, D. A. (1990) α-Helical coiled coils and bundles. How to design an α-helical protein. *Proteins* **7,** 1–15
13. Conway, J. F., and Parry, D. A. (1990) Structural features in the heptad substructure and longer range repeats of two-stranded α-fibrous proteins. *Int. J. Biol. Macromol.* **12,** 328–334
14. Graddis, T. J., Myszka, D. G., and Chaiken, I. M. (1993) Controlled formation of model homo- and heterodimer coiled coil polypeptides. *Biochemistry* **32,** 12664–12671
15. O'Shea, E. K., Lumb, K. J., and Kim, P. S. (1993) Peptide "Velcro." Design of a heterodimeric coiled coil. *Curr. Biol.* **3,** 658–667
16. Gonzalez, L., Jr., Woolfson, D. N., and Alber, T. (1996) Buried polar residues and structural specificity in the GCN4 leucine zipper. *Nat. Struct. Biol.* **3,** 1011–1018
17. Tripet, B., Wagschal, K., Lavigne, P., Mant, C. T., and Hodges, R. S. (2000) Effects of side-chain characteristics on stability and oligomerization state of a *de novo*-designed model coiled-coil. 20 amino acid substitutions in position "d." *J. Mol. Biol.* **300,** 377–402
18. Campbell, K. M., and Lumb, K. J. (2002) Complementation of buried lysine and surface polar residues in a designed heterodimeric coiled coil. *Biochemistry* **41,** 7169–7175
19. Campbell, K. M., Sholders, A. J., and Lumb, K. J. (2002) Contribution of buried lysine residues to the oligomerization specificity and stability of the fos coiled coil. *Biochemistry* **41,** 4866–4871
20. McClain, D. L., Gurnon, D. G., and Oakley, M. G. (2002) Importance of potential interhelical salt-bridges involving interior residues for coiled-coil stability and quaternary structure. *J. Mol. Biol.* **324,** 257–270
21. Chen, Y., Sharp, Z. D., and Lee, W. H. (1997) HEC binds to the seventh regulatory subunit of the 26 S proteasome and modulates the proteolysis of mitotic cyclins. *J. Biol. Chem.* **272,** 24081–24087

22. Chen, Y., Riley, D. J., Zheng, L., Chen, P. L., and Lee, W. H. (2002) Phosphorylation of the mitotic regulator protein Hec1 by Nek2 kinase is essential for faithful chromosome segregation. *J. Biol. Chem.* **277,** 49408–49416
23. Wu, G., Lin, Y. T., Wei, R., Chen, Y., Shan, Z., and Lee, W. H. (2008) Hice1, a novel microtubule-associated protein required for maintenance of spindle integrity and chromosomal stability in human cells. *Mol. Cell. Biol.* **28,** 3652–3662
24. Zheng, L., Chen, Y., and Lee, W. H. (1999) Hec1p, an evolutionarily conserved coiled-coil protein, modulates chromosome segregation through interaction with SMC proteins. *Mol. Cell. Biol.* **19,** 5417–5428
25. Chen, Y., Riley, D. J., Chen, P. L., and Lee, W. H. (1997) HEC, a novel nuclear protein rich in leucine heptad repeats specifically involved in mitosis. *Mol. Cell. Biol.* **17,** 6049–6056
26. Lin, Y. T., Chen, Y., Wu, G., and Lee, W. H. (2006) Hec1 sequentially recruits Zwint-1 and ZW10 to kinetochores for faithful chromosome segregation and spindle checkpoint control. *Oncogene* **25,** 6901–6914
27. Lupas, A., Van Dyke, M., and Stock, J. (1991) Predicting coiled coils from protein sequences. *Science* **252,** 1162–1164
28. Akey, D. L., Malashkevich, V. N., and Kim, P. S. (2001) Buried polar residues in coiled-coil interfaces. *Biochemistry* **40,** 6352–6360
29. Burkhard, P., Stetefeld, J., and Strelkov, S. V. (2001) Coiled coils. A highly versatile protein folding motif. *Trends Cell Biol.* **11,** 82–88
30. Havranek, J. J., and Harbury, P. B. (2003) Automated design of specificity in molecular recognition. *Nat. Struct. Biol.* **10,** 45–52
31. Bucher, P., Karplus, K., Moeri, N., and Hofmann, K. (1996) A flexible motif search technique based on generalized profiles. *Comput. Chem.* **20,** 3–23
32. Frank, S., Lustig, A., Schulthess, T., Engel, J., and Kammerer, R. A. (2000) A distinct seven-residue trigger sequence is indispensable for proper coiled-coil formation of the human macrophage scavenger receptor oligomerization domain. *J. Biol. Chem.* **275,** 11672–11677
33. Steinmetz, M. O., Stock, A., Schulthess, T., Landwehr, R., Lustig, A., Faix, J., Gerisch, G., Aebi, U., and Kammerer, R. A. (1998) A distinct 14 residue site triggers coiled-coil formation in cortexillin I. *EMBO J.* **17,** 1883–1891
34. Burkhard, P., Kammerer, R. A., Steinmetz, M. O., Bourenkov, G. P., and Aebi, U. (2000) The coiled-coil trigger site of the rod domain of cortexillin I unveils a distinct network of interhelical and intrahelical salt bridges. *Structure* **8,** 223–230
35. Kline, S. L., Cheeseman, I. M., Hori, T., Fukagawa, T., and Desai, A. (2006) The human Mis12 complex is required for kinetochore assembly and proper chromosome segregation. *J. Cell Biol.* **173,** 9–17
36. Régnier, V., Vagnarelli, P., Fukagawa, T., Zerjal, T., Burns, E., Trouche, D., Earnshaw, W., and Brown, W. (2005) CENP-A is required for accurate chromosome segregation and sustained kinetochore association of BubR1. *Mol. Cell. Biol.* **25,** 3967–3981
37. Kwon, M. S., Hori, T., Okada, M., and Fukagawa, T. (2007) CENP-C is involved in chromosome segregation, mitotic checkpoint function, and kinetochore assembly. *Mol. Biol. Cell* **18,** 2155–2168
38. McCleland, M. L., Kallio, M. J., Barrett-Wilt, G. A., Kestner, C. A., Shabanowitz, J., Hunt, D. F., Gorbsky, G. J., and Stukenberg, P. T. (2004) The vertebrate Ndc80 complex contains Spc24 and Spc25 homologs, which are required to establish and maintain kinetochore-microtubule attachment. *Curr. Biol.* **14,** 131–137
39. Panse, V. G., Hardeland, U., Werner, T., Kuster, B., and Hurt, E. (2004) A proteome-wide approach identifies sumoylated substrate proteins in yeast. *J. Biol. Chem.* **279,** 41346–41351
40. Wohlschlegel, J. A., Johnson, E. S., Reed, S. I., and Yates, J. R., 3rd (2004) Global analysis of protein sumoylation in *Saccharomyces cerevisiae*. *J. Biol. Chem.* **279,** 45662–45668
41. Zhou, W., Ryan, J. J., and Zhou, H. (2004) Global analyses of sumoylated proteins in *Saccharomyces cerevisiae*. Induction of protein sumoylation by cellular stresses. *J. Biol. Chem.* **279,** 32262–32268
42. Denison, C., Rudner, A. D., Gerber, S. A., Bakalarski, C. E., Moazed, D., and Gygi, S. P. (2005) A proteomic strategy for gaining insights into protein sumoylation in yeast. *Mol. Cell. Proteomics* **4,** 246–254
43. Hannich, J. T., Lewis, A., Kroetz, M. B., Li, S. J., Heide, H., Emili, A., and Hochstrasser, M. (2005) Defining the SUMO-modified proteome by multiple approaches in *Saccharomyces cerevisiae*. *J. Biol. Chem.* **280,** 4102–4110
44. Wykoff, D. D., and O'Shea, E. K. (2005) Identification of sumoylated proteins by systematic immunoprecipitation of the budding yeast proteome. *Mol. Cell. Proteomics* **4,** 73–83